Performance analysis of a novel thermal management system with composite phase change material for a lithium-ion battery pack

Xiaoming Wang[a], Yongqi Xie[a,*], Rodney Day[b], Hongwei Wu[b],

Zhongliang Hu[c], Jianqin Zhu[d], Dongsheng Wen[a,c*]

[a]School of Aeronautic Science and Engineering, Beihang University, Beijing, 100191, China

[b]School of Engineering and Technology, University of Hertfordshire, Hatfield, AL10 9AB, United Kingdom

[c]School of Chemical and Engineering, University of Leeds, Leeds, LS1 9JT, United Kingdom

[d]National Key Laboratory of Science and Technology on Aero-Engine Aero-thermodynamics, School of Energy and Power Engineering, Beihang University, Beijing 100191, China

[*]Corresponding author. Email: xyq@buaa.edu.cn d.wen@buaa.edu.cn Tel. (86)10-82338081

Abstract

A novel passive thermal management system (TMS) based on copper foam and paraffin composite phase change material (PCM) was designed for a lithium-ion battery pack in this work, where the phase change storage energy unit (PCSEU) was indirectly in contact with the cell. A combined experimental and numerical study was performed to investigate the thermal performance of the battery pack with the novel TMS and air cooling system (ACS). The effects of the PCSEU casing, PCM effective thermal conductivity, geometric structure parameters of the TMS, charge/discharge rate and ambient temperature were systematically evaluated, as well as the battery thermal behaviors during charge and discharge cycles. Results showed that the passive TMS could keep the battery temperature in a desirable range even under 4C discharge rate at 42 ^{o}C and the PCSEU casing could remarkably improve its heat absorption efficiency. The thickness of the heat conducting sheet demonstrated the greatest impact on the battery temperature. Pure ACS with an air flow rate $\leq$200 m^3/h could not meet the battery cooling demands. The passive TMS could achieve up to 3 cycles of 4C charge and discharge at 35 ^{o}C while keeping the maximum temperature of the battery pack below 52 ^{o}C.

Keywords: Lithium-ion battery; thermal management system; phase change material; metal foam; charge and discharge cycle

Nomenclature

a	Constant

A	Heat exchange area, m^2
c	Specific heat, J/(kg·K)
h	Convective heat transfer coefficient, W/(m^2·K)
H	Enthalpy, J/K
q	Heat generation rate of battery, W
t	Time, s
T	Temperature, K
V	Volume, m^3
γ	Latent heat, J/kg
β	Liquid fraction
ρ	Density, kg/m^3
λ	Thermal conductivity, W/(m·K)

Subscripts

a	Air
amb	Ambient
c	Battery cell
l	Liquid
p	Phase change material
ref	Reference
s	Solid
total	Total

Acronyms

ACS	Air cooling system
EG	Expanded graphite
EV	Electric vehicle
HEV	Hybrid electric vehicle
PCM	Phase change material
PCSEU	Phase change storage energy unit
TMS	Thermal management system

1. Introduction

Hybrid electric vehicle (HEV) and electric vehicle (EV) technologies have recently received intensive attentions from the public, governments and automotive companies in an effort to reduce greenhouse gas emission and air pollution, as well as noise level. It is also recognized that renewable energy technology usage is increasing in demand for such vehicles [1, 2]. Lithium-ion battery, a promising renewable energy storage unit with high energy density, high power capacity, low self-discharge and long lifespan, is considered to be one of the best power sources for HEV and EV [3]. However, a critical problem for the lithium-ion battery application is the large amount of heat generated, especially under off-normal conditions, which would lead to battery overheating, resulting in power fading or thermal runaway [4, 5].

It is noted that both the battery temperature and temperature distribution significantly affect the performance and lifespan of the battery. It is therefore imperative to find a proper thermal management system (TMS) to maintain the battery temperature within the desirable range. Numerous investigations on the battery thermal management have been performed by using air cooling [6, 7] and liquid cooling [8-10]. For example, Wang et al. [6] performed a numerical study and confirmed that increasing the inlet air velocity could achieve a lower temperature rise of the battery module, while higher air velocity and staggered cell arrangement would lead to a more even temperature distribution in the module. Saw et al. [7] carried out a steady state simulation and analyzed the thermal performance of the battery pack under different mass flow rates of the cooling air. They proposed that the cold spots and hot spots in the battery pack were able to be predicted and both the heat transfer coefficient and pressure drop could increase with an increase of the cooling air flow rate. Li et al. [8] performed a combined experimental and numerical study on the thermal performance of the water cooling based TMS. They stated that the active water cooling system could be a preferred approach to improve the thermal behavior of the battery pack at low cycling rates. Based on a two-dimensional transient model for the battery thermal management, Liu et al. [9] numerically investigated the effects of ambient temperature, Reynolds number and discharge rate on the battery temperature distribution using different cooling materials such as air, silicone oil and phase change material (PCM). It was found that the liquid cooling was more efficient to decrease temperature than

PCM cooling. However, the PCM cooling could result in more homogeneous temperature distribution. Although the above two cooling methods showed advantages in some aspects, additional components such as a pump, fan or heat sink makes them cumbersome with an extra increase of overall weight and cost. As a passive thermal management approach, PCMs integrated into a battery TMS have received increasing attention in recent years due to their compact structure, high efficiency and large latent heat, which can keep the temperature almost constant without consumption of extra energy [11-14].

There are many various types of PCMs that can be used for energy storage [15, 16]. As one of the most widely used organic PCMs, n-paraffin wax with a nearly constant phase change temperature, stability and non-corrosiveness is more suitable for battery thermal management [2, 11, 17]. Al-Hallaj and Selman [18] firstly proposed a PCM-based TMS for a large scaled battery pack and numerically investigated the thermal behavior of the battery pack. It was reported that the PCM could maintain the battery temperature effectively without an external power source. However, the low thermal conductivity of a pure PCM would substantially impede the complete exertion of its cooling potential.

In order to overcome the problem mentioned above, a variety of approaches aiming to improve the thermal conductivity of PCMs were developed by suspending thermally conductive fillers (such as nanoparticles [19], carbon nanotubes), embedding PCM into porous media (such as metal foam [12, 20], expanded graphite (EG) [21]), attaching metal meshes [13] or fins [22]. Using a matrix with micro-composite graphite and PCM surrounding the array of cells, Sabbah et al. [23] compared the effectiveness of the PCM thermal management with that of forced air cooling for high power batteries. Their results indicated that PCM-based TMS could keep the cell temperature within the battery pack less than 55 ^{o}C when the constant discharge rate was as high as 6.67 C under ambient temperature of 45 ^{o}C or higher. But the forced air cooling was unable to maintain the cell temperature below 55 ^{o}C. Wang et al. [24] investigated experimentally the heat storage properties of the pure paraffin and paraffin/aluminum foam composite PCM under different heat fluxes. It was found that the composite PCM had an ideal cooling effect on suppressing the battery temperature rise during the discharge. Wu et al. [25] designed a pyrolytic graphite sheets-enhanced paraffin/EG composites based TMS and a good temperature distribution under dynamic cycles and failure

mode for a large-format lithium-ion battery was achieved. The composite PCM was filled in the gap between the cells. They found that the enhanced paraffin/EG composite based TMS showed much better cooling performance and temperature uniformity compared to paraffin/EG TMS during five charge/discharge cycles. A coupled battery TMS using a novel quaternary PCM plate was developed by Situ et al. [26]. Four different materials such as paraffin, EG, low density polyethylene and double copper mesh were combined into the quaternary PCM plate. The thermal conductivity of the PCM plate with double copper mesh was increased by 36% in comparison to that of PCM plate composed of paraffin and EG alone. Their results revealed that the PCM plate with double copper mesh reduced the maximum temperature and the maximum temperature difference inside the battery module to below 52.8 ^{o}C and 3 ^{o}C, respectively. Alipanah and Li [27] numerically simulated the surface temperature and discharge time of the lithium-ion battery with three different TMSs using pure gallium, pure octadecane and octadecane/aluminum foam composite. It was observed that before the battery average surface temperature over 60 ^{o}C, a thicker TMS caused a longer discharge time as the PCM could absorb more heat. Adding aluminum foam into the octadecane obviously increased the discharge time and reduced the battery surface temperature. A passive TMS based on the copper foam and paraffin composite PCM for high power lithium-ion battery was designed and experimentally studied by Li et al. [12]. It was concluded that the melting of PCM occurred at above 1C discharge rate and the battery temperature was within the safety temperature for pure PCM and composite PCM. Moreover, the composite PCM could cause a lower battery temperature and more uniform temperature distribution. Malik et al. [28] designed a passive TMS for lithium-ion battery pack utilizing PCM and experimentally studied the thermal performance under different discharge rates and thicknesses of PCM plate. For 6 mm thick PCM plate, the battery surface temperature decreased from 56.5 ^{o}C with no cooling to 36.5 ^{o}C at 4C discharge. As the thickness of PCM plate was more than 6 mm, the impact of increasing PCM thickness on the battery temperature was insignificant. Zhao et al. [29] proposed a PCM based battery internal cooling system using a PCM-filled mandrel to replace the hollow mandrel in cylindrical battery. The design was optimized by comprehensively analyzing PCM species and PCM core size. Their results indicated that the PCM core could effectively restrain the temperature rise in the battery pack. Thicker PCM core led to a more uniform temperature

distribution.

To the best of author's knowledge, the search for compact, efficient and reliable TMS for battery pack is still going on although some progress has been made. Moreover, almost all previous research on the PCM-based TMS were mainly focused on directly filling PCMs into the space among the battery cells. Clearly in this way, the quantity of usable PCMs is constrained by the space available. In addition, a higher thermal resistance would occur between the cells and heat sink after the complete melt of PCMs , which may produce a thermal insulation effect on the battery cells, decreasing significantly the heat dissipation performance. On the other hand, there is still much scope for metal foam and PCM composite thermal management for lithium-ion power battery, especially for the investigations of the influence of geometric structure parameters, charge/discharge rate and ambient temperature on the thermal behavior of the battery pack. Thus, the current work aims to develop a novel indirect cooling TMS with copper foam and paraffin composite PCM for a pouch lithium-ion battery pack. The phase change storage energy unit (PCSEU) in the system was indirectly in touch with the cells. Another major contribution could be to study the effect of PCSEU casing, geometric structure parameters and ambient temperature on the thermal behavior of the battery pack under high charge/discharge rate conditions.

In this article, a combined experimental and numerical investigation on the thermal characteristics of the novel composite PCM-based TMS was carried out. The effects of various influential factors, such as PCSEU casing, geometric structure parameters, effective thermal conductivity of composite PCM, charge/discharge rate and ambient temperature on the battery temperature were analyzed in a systematic manner. Furthermore, the thermal performances of the battery pack during charge and discharge cycles were evaluated for the air cooling-based TMS and composite PCM-based TMS.

2. Experimental setup

In the current work, a new experimental rig was set up at Human-Machine and Environmental Engineering (HMEE) Laboratory at Beihang University, China to investigate the charge/discharge and thermal management performance of the lithium-ion battery pack with the composite PCM-based TMS.

2.1 Experimental apparatus

Fig. 1 illustrates a schematic diagram of the battery charge/discharge and thermal performance experimental test rig. The experimental system mainly consisted of the battery charge/discharge subsystem, thermal performance test subsystem and test section. The charge/discharge subsystem included control software and program- controlled DC power supplies and . This subsystem was used to simulate the battery operation at different charge and discharge rates. For the discharge process, the battery was discharged to 18 V with constant currents of 2C (20A), 3C (30A) and 4C (40A). While for the charge process, the battery was firstly charged with constant current until the terminal voltage reached 33.6 V, and then charged to 0.05 A with constant voltage of 33.6 V. The thermal performance test subsystem was mainly composed of an Agilent 34970A data acquisition unit, a thermostatic chamber (QGT302P), and eight platinum temperature sensors (PT100) with accuracy of ±0.06 ^{o}C at 0 ^{o}C. The thermostatic chamber was utilized to maintain different surrounding temperatures. Three temperatures of 28 ^{o}C, 35 ^{o}C and 42 ^{o}C were selected as the operating temperature. Six temperature sensors were placed on the surface of three different cells inside the battery pack where two PT100 probes were affixed on the side surface of the cell. Another two PT100 probes were affixed on the outside surface of the PCSEUs. All of the test temperatures were recorded every second by the Agilent 34970A data acquisition unit.

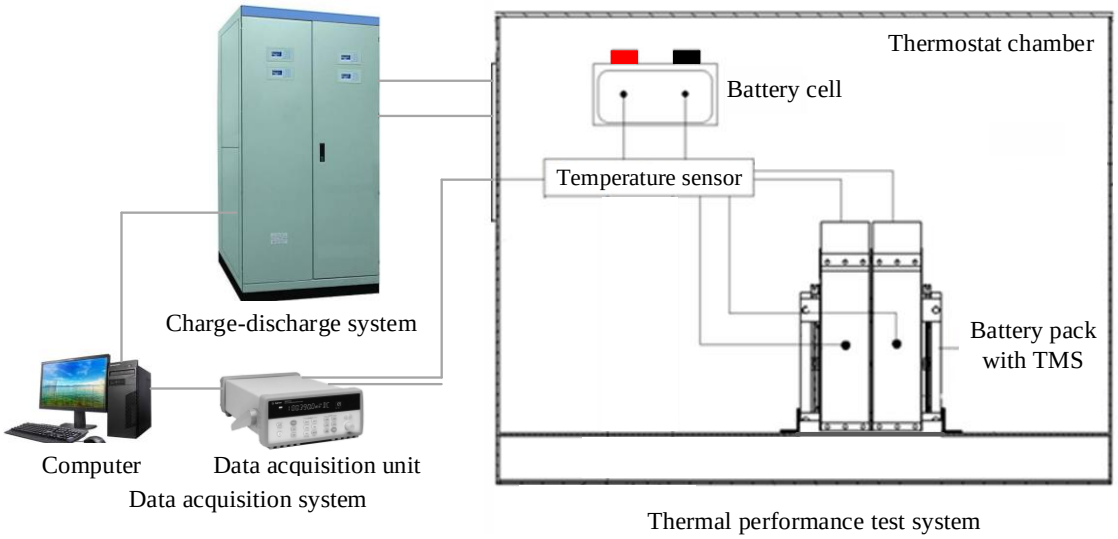

Fig. 1. The battery charge/discharge and thermal performance experimental system.

The test section was the lithium-ion titanate battery pack that comprised of twelve single battery cells. Table 1 lists the specific parameters of the lithium-ion battery. Each single cell

was comprised of a battery core, porous structure frame and 0.35 mm thick aluminum sheet. The aluminum sheet was used to protect the cell from being damaged. The test section was placed vertically inside the thermostatic chamber.

During the experiments, the required battery working environment was provided by using the thermostatic chamber firstly. The battery was then charged or discharged at a specified rate by the charge/discharge subsystem. At the same time, the temperature of the battery, PCSEUs and ambient temperature as well as charge/discharge voltage and current were recorded and saved accordingly.

Table 1 Specific parameters of commercial lithium-ion battery

Specifications	Value (unit)
Battery type	Lithium-ion titanate battery
Cell dimensions	6.1 mm×203 mm×127 mm
Nominal voltage	2.3 V
Nominal capacity	10 Ah
Recommended operation temperature	-10 ~ +45 ºC (charge) -25 ~ +55 ºC (discharge)
Thermal conductivity of battery cell*	5.22 W/(m·K)

*it is an average value of measured thermal conductivity for cells

2.2 Design description of the TMS

When taking the safety, structure and weight limits into accounts, a novel composite PCM-based TMS was designed to dissipate the heat generated in the battery pack. Fig. 2 depicts the schematic and picture view of this novel TMS. Different from the common configuration of filling the PCMs in the gap between the cells, two different PCSEUs, namely PCSEU-1 and PCSEU-2, were arranged in parallel on a L-shape collector plate outside the battery pack. This special arrangement not only avoided the PCMs directly contacting the battery cell but also could utilize more PCMs for heat absorption without occupying the battery pack space. The PCSEU-1 with the size of 120 mm×30 mm×46 mm was installed at the far end of the collector plate, which was the upper one shown in Fig. 2. The PCSEU-2 with the

size of 145 mm×45 mm×46 mm was closer to the battery cells, which was the side one shown in Fig. 2.

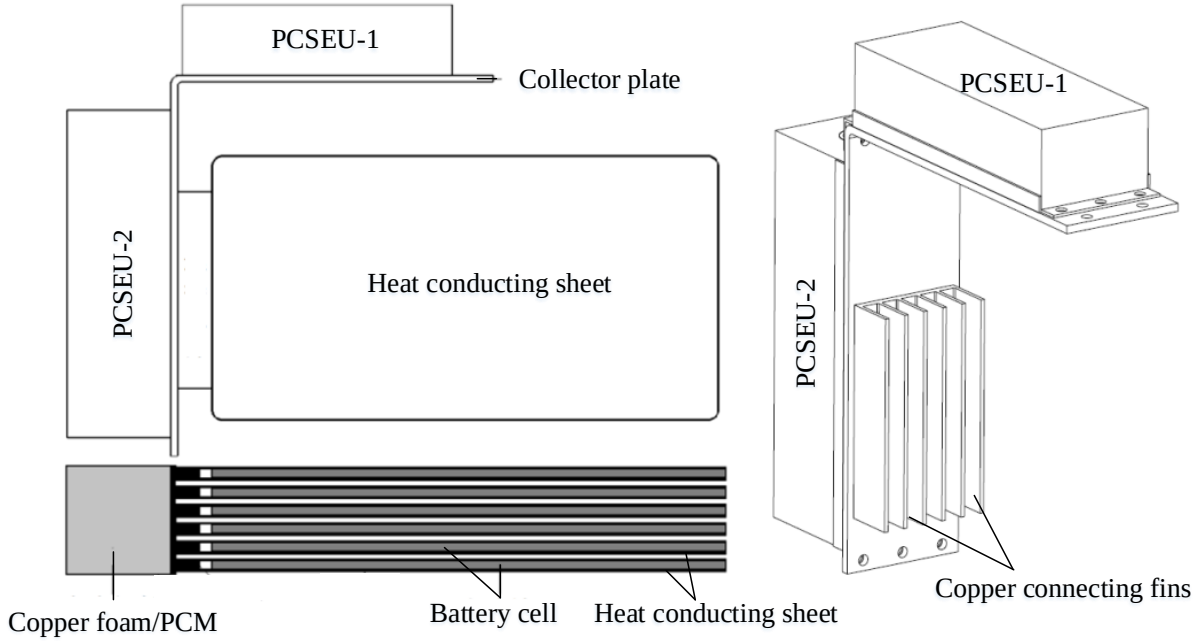

(a) Schematic of the TMS

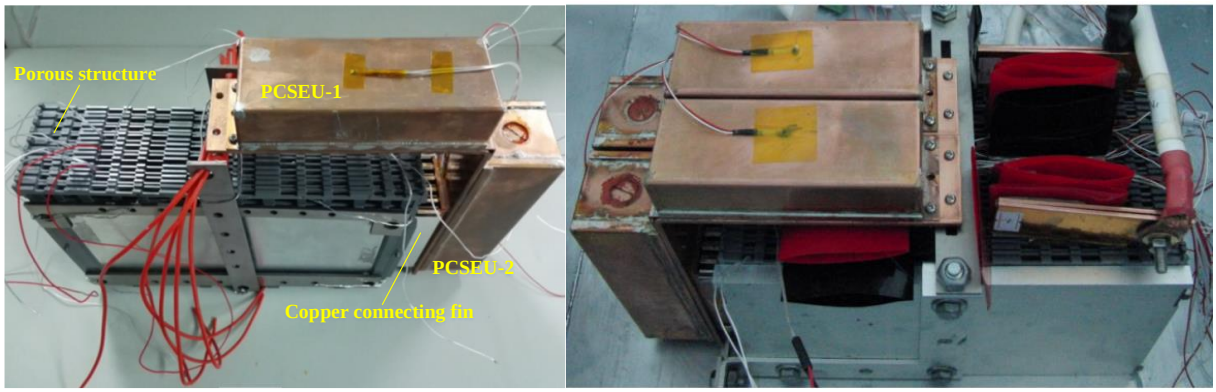

(b) Battery pack assembled the TMS

Fig. 2. The schematic view of the TMS and battery pack assembled the TMS.

The core of the PCSEU was made of copper foam with porosity of 95% and n-eicosane paraffin with purity of 99%, which was packaged by 1 mm thick copper plate. The copper foam had the advantage of being light-weight with a large surface area and thermal conductivity. Padding with copper foam could significantly increase the thermal conductivity and heat storage efficiency of the paraffin. In order to reduce the contact thermal resistance, welding was used to link the copper foam and copper plate. The paraffin was impregnated into the copper foam by a vacuuming procedure. During the perfusion, the paraffin was heated to

fully melting and then kept at approximate 55 ^{o}C to diminish the swelling stress generated by the volume expansion of the melted PCM. When the perfusion was finished, the unit was sealed immediately.

The melting point of the n-eicosane paraffin is 36.0~38.0 ^{o}C, which is one to three degrees higher than the ambient temperature of 35 ^{o}C during the summer. It contributes to decreasing the heat transfer between the PCMs and surroundings as phase change occurs. The latent heat of the paraffin is 241 kJ/kg with thermal conductivity of 0.274 W/(m·K) and density of 788.6 kg/m^3. A Hot Disk Analyzer (TPS 1500) based on the transient plane source method [30] was used to measure the thermal conductivity and specific capacity of the composite PCM, which were 5.28 W/(m·K) and 1.634 kJ/(kg·K), respectively.

In the TMS, the aluminum sheet of the battery cell was used as the heat conducting sheet. This would simplify the system structure and eliminate the cell damage risk when assembling an additional sheet. Since the sheet thickness was only 0.35 mm, thermal accumulation could easily be introduced if the sheet directly linked the collector plate. Thus, copper connecting fins were utilized to reduce the thermal resistance between the sheet and the collector plate. The thickness of the connecting fin was 1.5 mm and the height was 15 mm. The copper collector plate with a thickness of 4 mm was used to collect the heat from the cells and install the PCSEUs. The length and width of the L-shape plate assembled with the PCSEU-2 was 160 mm and 50 mm, respectively, whereas the size of the plate assembled with the PCSEU-1 was 135 mm and 50 mm, respectively. When the battery charged or discharged, the heat generated inside the battery was transferred to the PCSEUs from the cells through the heat conducting sheet, connecting fin and collector plate.

2.3 Battery heat generation rate

The heat generation depended on the battery internal resistance and the charge/discharge rate. It basically consisted of irreversible Joule heat, reversible heat from the electrochemical reactions, heat from side reactions and heat of mixing [31, 32]. Based on the heat transfer analysis of the battery [33], the heat generation rate (q) could be obtained as follows.

$$q = hA\left(\frac{T - T_0}{1 - \exp\left(-\frac{hA}{\rho_c c_c V_c} t\right)} + T_0 - T_{amb}\right) \quad (1)$$

where h is the convective heat transfer coefficient, A is the heat exchange area, t is the time, T and T_0 are the battery temperature at the time of 0 and t, T_{amb} is the ambient temperature, ρ_c is the density of the cell, c_c is the specific heat of the cell and V_c is the volume of the cell.

For different charge/discharge rates and ambient temperatures, the heat generation rate at a given time could be determined by Eq. (1) and the related experimental data in term of the battery temperature drop. In order to facilitate the calculation of the heat generation rate in the simulations, the following polynomial expression for the cases of 4C charge/discharge rate and 35 ^{o}C was fitted by utilizing the least square method.

$$q = a_0 + a_1 t + a_2 t^2 + \cdots + a_n t^n \ , n = 1,2,\cdots, t \le t_{total} \quad (2)$$

where q is the heat generation rate of the battery, t is the time, a_0, a_1, $\cdots$, a_n are constant for a given charge/discharge rate and ambient temperature.

When n was equal to 7, the polynomial fitting R-square was more than 0.988, which indicated that the curve was matching well with the calculation value of the heat generation. Table 2 gives the coefficient of the polynomial fitting for the case of 4C charge and discharge at 35 ^{o}C.

Table 2 Coefficient of polynomial fitting at 4C charge/discharge and 35 ^{o}C

Condition	a_0	a_1	a_2	a_3	a_4	a_5	a_6	a_7
4C discharge	-3.7375	0.6863	-0.0133	1.1742E-4	-5.6878E-7	1.6347E-9	-2.8544E-12	2.9673E-15
4C Charge	0.1119	0.3846	-0.0071	5.1582E-5	-2.8953E-10	7.8784E-10	-1.2799E-12	1.2271E-15

3. Numerical analysis

3.1 Model setup

A simplified physical model of the battery pack with composite PCM based TMS was developed and the computational domain was consistent with the test geometry. Hexahedral elements were generated using commercial software ICEM CFD 14.0, as shown in Fig. 3. In order to address the distinction from the thermal performance of pure air cooling system (ACS),

the corresponding simulation model including the battery cells and air was constructed as well.

In order to reduce the thermal contact resistance, thermal grease with thermal conductivity of 4.8 W/(m·K) was utilized between the PCSEUs and collector plate. Thus, the related layer with the thickness of 0.1 mm was added in the physical model. For other contact interfaces, perfect contacts were assumed. The physical properties of the battery cell and TMS were listed in Table 3.

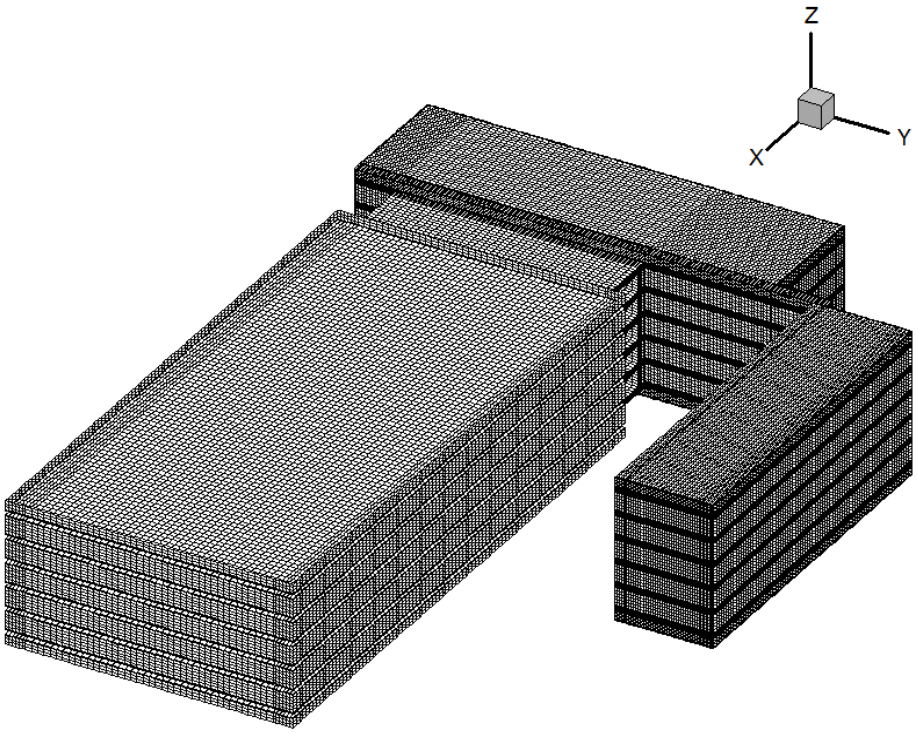

Fig. 3 The computational domain and grid of the battery pack with the TMS

Table 3 The physical properties of the battery cell and TMS

Material	ρ	c	λ	γ
Battery cell	2857	1287	5.22	-
Composite PCM	1019	1634	5.28	135
Copper	8441	386	377	-
Aluminum	2719	871	202	-

Prior to implementation of the simulation, grid independence analyses for the model were performed by utilizing different numbers of grids with 362,415, 581,357, 963,363, 1,656,798, respectively. The battery temperature was predicted as the ambient temperature was 35^{o}C and the constant heat generation rate was set to 5 W. The maximum variation of the battery maximum temperature was 0.42% when the grid number was increased from 963,363 to

1,656,798, while a maximum of 1.52% was observed as the grid number was increased from 581,357 to 963,363. Therefore, a compromise between computation accuracy and computing capability led to the use of 963,363 grids.

3.2 Governing equation

For the copper foam and paraffin composite PCM, the heat storage process could be considered as a relatively slow heat conducting process. The mathematical model describing the composite PCM phase change process was similar to that of pure paraffin [34]. In the present study, the radiation heat transfer was ignored due to relatively low battery temperature [35]. The heat transfer between the battery pack and surroundings was also neglected. The properties of the composite PCM were assumed to be constant and equal for both liquid and solid phase [35, 36]. The motion of the solid paraffin, the volume variation and the convective heat transfer between the copper foam and paraffin were all disregarded during the phase change process [37]. As a consequence, the melting of the composite PCM could be considered as pure heat conduction process.

Based on energy conservation and the above assumptions, the energy equation for the domain of the cells could be expressed by Eq. (3):

$$\rho_{\mathrm{c}} c_{\mathrm{c}} \frac{\partial T}{\partial t} = \nabla \cdot \left(\lambda_{\mathrm{c}} \nabla T \right) + q \tag{3}$$

where λ_{c} is the thermal conductivity of the cell.

For the domain of the PCM, since a pure heat conduction was considered when the PCM was melting or solidifying, the energy equation could be presented as follows:

$$\rho_{\mathrm{p}} \frac{\partial H}{\partial t} = \nabla \cdot \left(\lambda_{\mathrm{p}} \nabla T \right) \tag{4}$$

$$H = \int_{T_{\mathrm{ref}}}^{T} c_{\mathrm{p}} dT + \beta \gamma \tag{5}$$

where ρ_{p} is the density of the PCM, H is the enthalpy of the PCM, λ_{p} is the effective thermal conductivity of the PCM, γ is the latent heat of the PCM, and β is the liquid fraction of the PCM, which can be calculated as [35, 38]:

$$\beta = \begin{cases} 0 & T < T_{\mathrm{s}} \\ \left(T - T_{\mathrm{s}} \right) / \left(T_{\mathrm{l}} - T_{\mathrm{s}} \right) & T_{\mathrm{s}} < T < T_{\mathrm{l}} \\ 1 & T > T_{\mathrm{l}} \end{cases} \tag{6}$$

where T_s and T_l are the solidification and liquefaction temperature of the PCM, respectively.

For the fluid domain of the air in the ACS, the conservation equations of continuity, momentum and energy were given by Eqs. (7), (8) and (9), respectively.

$$\frac{\partial \rho_a}{\partial t} + \nabla \cdot (\rho_a \vec{u}) = 0 \tag{7}$$

$$\frac{\partial (\rho_a \vec{u})}{\partial t} + \nabla \cdot (\rho_a \vec{u}\vec{u}) = -\nabla p_a + \nabla \cdot \left(\mu_a \nabla \vec{u} + \mu_a \nabla \vec{u}^{T} \right) \tag{8}$$

$$\frac{\partial (\rho_a c_a T)}{\partial t} + \nabla \cdot (\rho_a c_a \vec{u} T) = \nabla \cdot (k_a \nabla T) \tag{9}$$

where ρ_a and c_a are the density and specific heat of the cooling air, $\vec{u}$ is the velocity vector of the cooling air, μ_a is the dynamic viscosity of the cooling air and p_a is the static pressure. Besides, the standard turbulent model, *k-ε* model, was employed to predict the flow behavior [29].

In order to examine the thermal behavior of the battery pack under severe conditions, a large charge and discharge rate of 4C was selected for this purpose. Both charge and discharge times were approximately 900 s. The initial temperatures of the cells and the PCSEUs were equal to the ambient temperature. The time step was set as 1 s and the iteration number per time step was 50. For the continuity, momentum and energy equations, the convergence criteria were set to 1×10^{-4} of the residuals. The commercial software ANSYS FLUENT 14.0 was used to solve the above governing equations.

3.3 Model validation

In order to verify the phase change model of the PCM, an electric heater emulating the battery was designed to simulate the battery heat generation and the experiments were conducted at ambient temperature of 35 °C. A constant heat power was set to 5 W. The test section including the composite PCM-based TMS was placed in the thermostatic chamber where the natural convection heat transfer coefficient was estimated to be 5 W/m^2·K. The simulation results could illustrate the temperature distribution inside the battery and PCSEUs, but during the experiments, their surface temperatures can only be measured. Therefore, the comparison of the experimental and simulated surface temperatures of the battery, PCSEU-1 and PCSEU-2 is presented in Fig. 4.

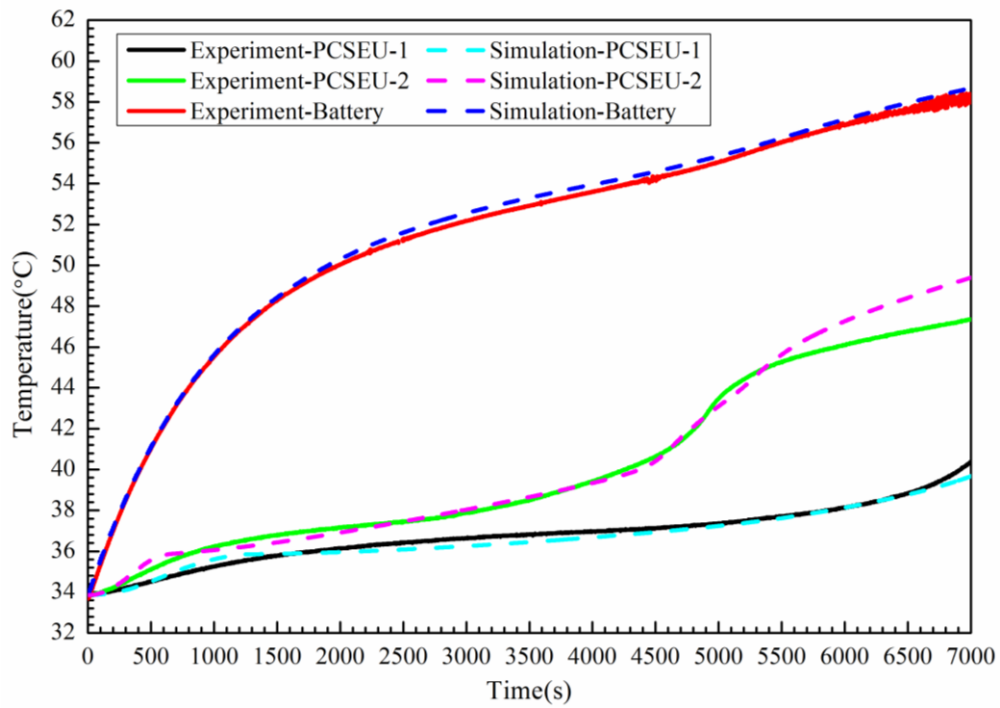

Fig. 4 Comparison of the experimental and simulated results for the battery and TMS

From Fig. 4, it can be observed clearly that the surface temperatures of the battery and PCSEUs showed a similar trend under both experimental and computational conditions. Overall, the maximum error was not more than 5%. The computed results were in good agreement with the experimental data, which indicated that the phase change model was robust and accurate.

Furthermore, the heat generation of the battery was critical to achieve accurate simulation results. For the purpose of validating the heat generation rate of the battery, the actual battery pack was used, as shown in Fig. 2. Both the simulation and experiment on the temperature of the battery pack with the composite PCM-based TMS were conducted under 4C charge/discharge rates and natural convection conditions. The heat transfer coefficient was set to be 5 $W/m^2 \cdot K$. The ambient temperature was 35 ^oC. Fig. 5 depicts the comparison of the battery surface temperature between experimental data and simulated results.

As shown in Fig. 5, it can be clearly seen that the simulated temperature was in good agreement with experimental measurements. The maximum error was 1.3% in 4C discharge process whereas 2.1% in 4C charge process. The results demonstrated that the heat generation rate model could accurately calculate the heat generation of the battery.

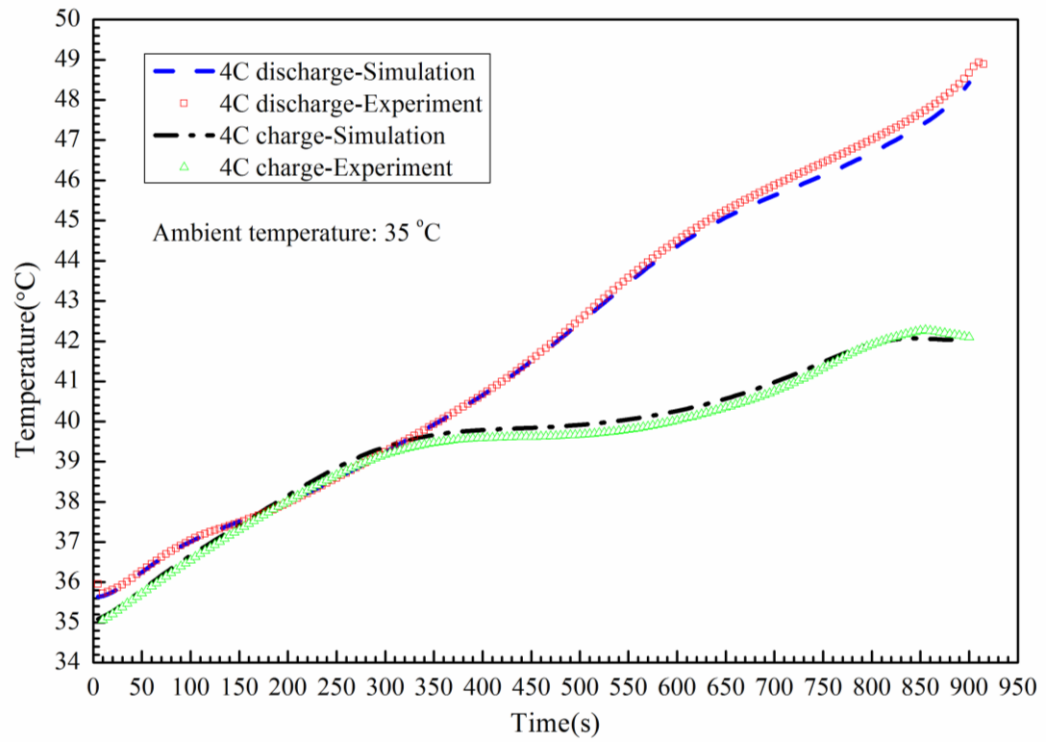

Fig. 5. Comparison of experimental and simulated battery surface temperatures at 4C charge/discharge rates and 35 °C.

4. Results and discussion

4.1 Impact of PCSEU casing

The composite PCM casing was required to prevent the potential leakage of the liquid PCM. Metal material with high thermal conductivity was used as the casing to improve the heat transfer performance. It should be noted here that most of previous studies were focused on the thermal behavior of the composite PCM with less attention paid to the impact of the casing on the heat transfer performance of PCM, as described below.

Fig. 6 shows the liquid fraction distribution of the PCMs with and without copper casing during melting. The endothermic capacity of the PCM was associated with its liquid fraction, which is an important index representing the phase change progress and effectiveness of the PCM itself. As can be seen from Fig. 6, there was an obvious difference for the liquid fraction distribution at different time between with and without casing. The impact of the casing on the melting process in the PCSEU-2 was greater than that in the PCSEU-1.

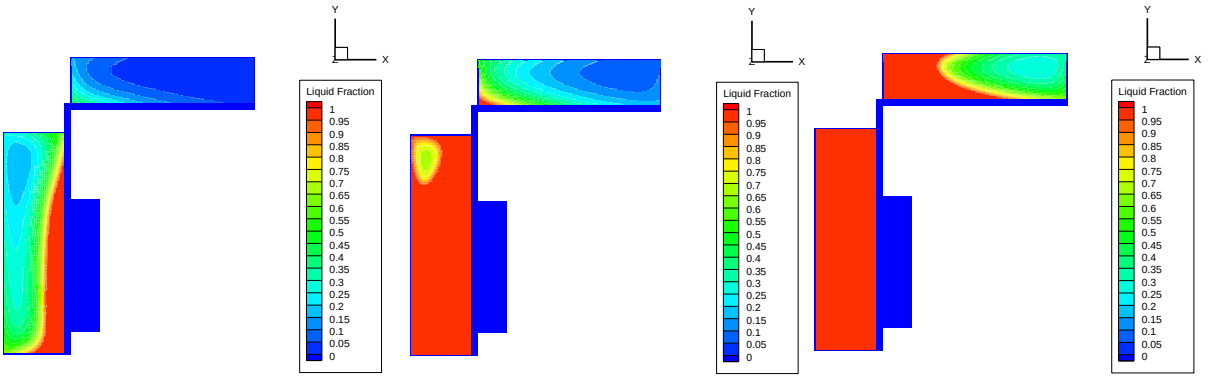

(a) 2500 s-With casing (b) 4000 s-With casing (c) 5500 s-With casing

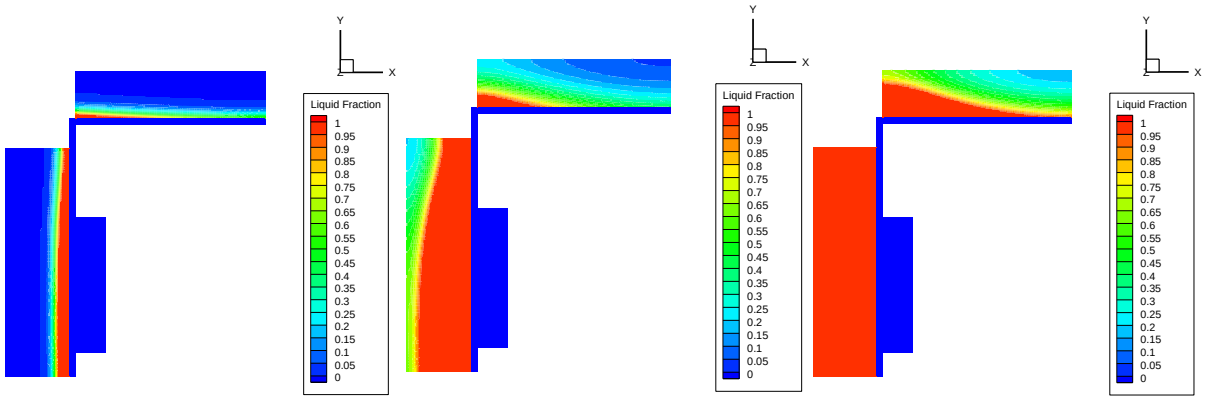

(d) 2500 s-Without casing (e) 4000 s-Without casing (f) 5500 s-Without casing

Fig. 6 Liquid fraction distribution for composite PCM with and without copper casing

For the case of with casing, as shown in Fig. 6(a)-(c), the heat was transferred through and around the walls to the centre as due to the large thermal conductivity of the copper casing. The PCM near the copper casing was firstly melted and the solid-liquid interface moved to the centre gradually. The heat absorption efficiency of the composite PCM was increased by the copper casing. At 2500 s, the liquid fraction was less than 1 in most areas inside PCSEU-2, which indicated that most PCMs had melted. However, a majority of PCMs did not melt inside PCSEU-1. At 4000 s, most of PCMs inside PCSEU-2 melted completely. At 5500 s, all PCMs inside PCSEU-2 was melted completely and a majority of the PCMs inside PCSEU-1 was melted.

For the case of without casing, as shown in Fig. 6(d)-(f), the heat was transferred from the wall near the heat source to the opposite by the aid of the fiber structure of copper foam. Obviously, stratified melting of the PCMs existed. Before 2500 s, most of the PCMs inside both PCSEU-1 and PCSEU-2 did not melt. At 4000 s, most of the PCMs inside PCSEU-2 fully melted, whereas only part of PCMs was melted inside PCSEU-1. It was observed that at 5500 s

the PCM inside PCSEU-2 completely melted.

The experimental results of the surface temperature of both the battery and PCSEUs with and without casing also supported the above conclusions, as shown in Fig. 7. The heat power of the electric heater was 5 W. It could be found from Fig. 7 that the time period for the maximum difference in the temperature curves of the battery was from 2000 s to 4500 s. During this period, the PCMs inside the PCSEU-2 did not fully melt. Owing to the smaller thermal resistance between the heat source and PCSEU-2, the copper casing improved the heat transfer and reduced the battery temperature. Due to the larger thermal resistance between the heat source and PCSEU-1, the casing had no significant effect on the temperature of the heat source.

As a consequence, the PCSEU casing could improve the heat transfer of the composite PCM and decrease the battery temperature. It is suggested that the casing material with large thermal conductivity should be adopted. The impact of PCSEU casing on the melting process should be taken into account in the simulation when the total thermal resistance between the PCM and the battery cell was small.

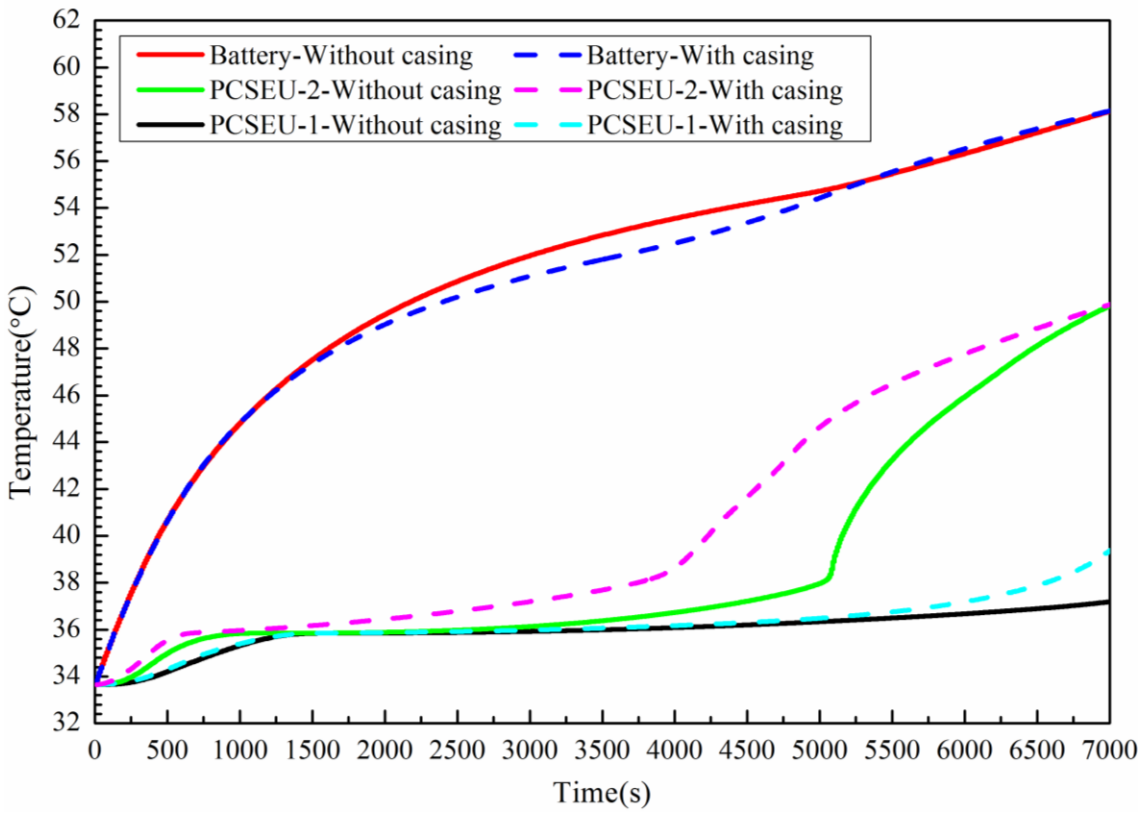

Fig. 7 Temperature profiles of the battery and PCSEUs with and without copper casing

4.2 Impact of PCM thermal conductivity

In the current work, three different thermal conductivity values, i.e. 1.69, 3.94, 6.90 W/(m·K) were selected for assessing the impact of the composite PCM thermal conductivity on the battery thermal performance. Fig. 8 shows the maximum temperature of the battery at three different thermal conductivities under 4C discharge at constant ambient temperature of 35 ^{o}C. The liquid fraction β=0 denoted that the PCMs did not melt, whereas β=0.5 indicated that the PCMs almost melted completely inside the PCSEU-2 but not melted inside the PCSEU-1. β=1 denoted that the PCMs inside both PCSEUs completely melted. As shown in Fig. 8, the battery temperature increased with the increase of the liquid fraction for a given thermal conductivity. During the overall melting process, the battery temperature decreased with increasing thermal conductivity. For the composite PCM with high thermal conductivity, the thermal resistance during the melting process increased slightly. Therefore, the heat resulted from the battery easily diffused inside the composite PCM and then the heat accumulation inside the battery was removed. As a consequence, the battery temperature descended.

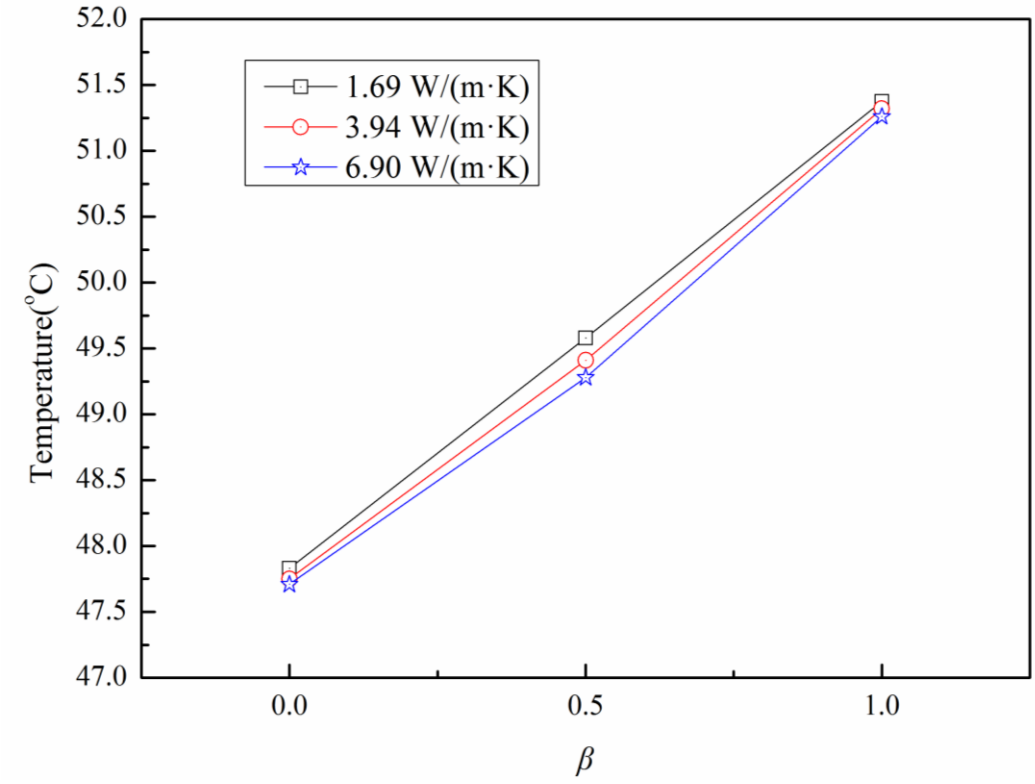

Fig. 8. Battery maximum temperature at different thermal conductivities and 4C discharge

It can also be found that the ratio of the battery temperature drop to the thermal conductivity rise was approximately 0.08 when the thermal conductivity increased from 1.69 W/(m·K) to

6.90 W/(m·K). This indicated that further increasing the thermal conductivity had insignificant impact on the battery temperature for large thermal conductivity. This result could be explained by the following reasons. Assuming that the thermal conductivity was very large, the temperature of the entire PCM during melting process was equal to the phase transition temperature. Under this condition, the thermal conductivity change could not affect the battery temperature. Moreover, since the Biot number was very small for the PCSEU, the temperature distribution inside the unit was approximately uniform and only dependent on the time. Compared to the external thermal resistance including heat conducting sheet, connecting fin and heat collector plate, the internal thermal resistance of the unit could be neglected. Therefore, increasing the thermal conductivity could not lead to obvious temperature drop of the battery. The similar results were also reported by Rao et al. [39].

On the other hand, the charge/discharge time was short for high charge/discharge rate although the heat generation rate was large. In the present study, the duration of 4C discharge was only 900 s. Furthermore, the melting mass of the PCM was small due to its large latent heat. Consequently, a small increase of the thermal resistance of the composite PCM was caused in a single discharge process. Therefore, increasing the thermal conductivity could not result in a remarkable drop of the battery temperature. It was worth highlighting that the effect of the thermal conductivity change on the battery temperature would become obvious for the battery with much longer working time.

In summary, increasing the thermal conductivity of the composite PCM contributed to decrease the battery temperature. When the thermal conductivity increased to a certain value, the effect of further increasing thermal conductivity on reducing the battery temperature was insignificant. Furthermore, increasing the thermal conductivity by enlarging the porosity of the copper foam potentially led to the decrease of the available quantity of the paraffin, which further shortened the working time of the PCMs. For the proposed indirect cooling system in the current study, the effects of the external thermal resistance and battery working time would be taken into account when increasing the thermal conductivity of the composite PCM.

4.3 TMS geometry parameter optimization

In the TMS, the total thermal resistance from the battery to the PCSEU, comprising heat conducting sheet, connecting fin and collector plate, remarkably affected the thermal

performance of the PCSEUs. Evaluating the ratio of the thermal resistance of each component to the total thermal resistance could improve the design of the TMS. Based on the current system structure, the key parameters were mainly the thickness of the collector plate, heat conducting sheet and connecting fin as well as the connecting fin height, respectively.

Using the control variate method, the impacts of the above four parameters on the battery temperature were analyzed in detail, as shown in Fig. 9. In the simulations, the battery heat generation was set to 5 W and the natural convective coefficient was set to 5 W/(m^2·K). It can be seen from Fig. 9 that the change of the heat conducting sheet thickness caused the most obvious variation of the battery temperature. The next was the change of the connecting fin height which led to an obvious variation of the battery temperature. It was noted, however, that changing the thickness of the collector plate and connecting fin resulted in a very small change of the battery temperature.

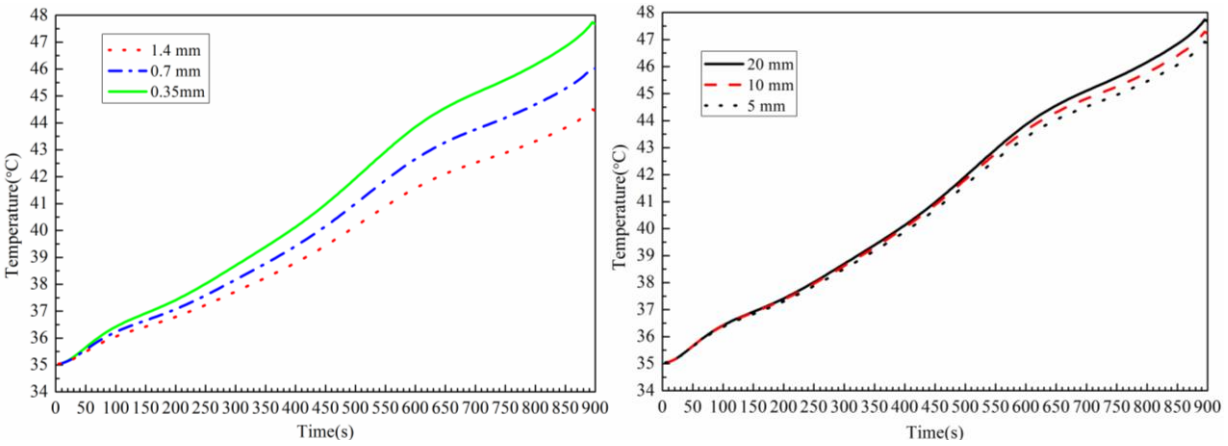

(a) heat conducting sheet thickness (b) connecting fin height

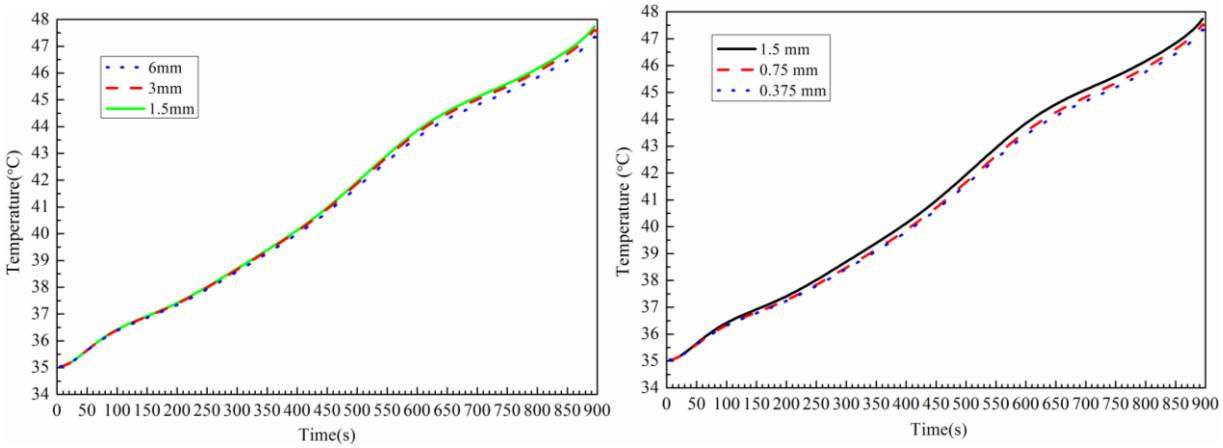

(b) connecting fin thickness (d) collector plate thickness

Fig. 9 The battery temperature change for different TMS geometry parameters

As the thickness of the heat conducting sheet increased, as shown in Fig. 9(a), the heat transfer area along the length direction of the sheet increased as well. At the same time, the thermal resistance along the thickness direction of the sheet also increased slightly. However, since the heat flux mainly transferred along the length direction, the effect of increasing the thermal resistance along the thickness direction on the heat transfer could be neglected. Therefore, according to Fourier's law, the battery temperature reduced as the thickness increased under the same heat absorption of the PCM. Reducing the height of the connecting fin decreased the thermal resistance from the battery to the PCSEUs. Thus, it could decrease the battery temperature, as shown in Fig. 9(b). However, the connecting fin height could not be less than 20 mm due to the structure constraints.

In Fig. 9(c), the battery temperature drop was not obvious as increasing the connecting fin thickness, although it enlarged the heat transfer area. The main reason could be that the heat conducting sheet thickness was very small and much less than the connecting fin thickness. It could be seen from Fig. 9(d) that the battery temperature changes were not obvious under different collector plate thickness. Enlarging the collector plate thickness could increase the heat transfer area of PCSEU-1, which would improve the heat transfer to PCSEU-1 and decrease the battery temperature. But for PCSEU-2, it increased the thermal resistance and prevented the heat to PCSEU-2. Under both combined actions, increasing the collector plate thickness had no significant impact in decreasing the battery temperature.

According to the above analysis, increasing the thickness of the heat conducting sheet could be the most efficient way to improve the cooling performance of the TMS. But it needs to be stressed here that the geometry constraints of the battery pack would also need to be taken into account.

4.4 Thermal performance of battery pack

4.4.1 Impact of different charge/discharge rates

The test temperature profiles of the battery pack during 3C and 4C charge/discharge under ambient temperature of 35 ^{o}C are depicted in Fig. 10. It could be found that the battery temperature during discharge process was remarkably higher than that during charge process. The temperature of the battery pack reached the maximum value at the end of 3C and 4C discharge. Due to the higher initial temperature in 3C discharge process, the maximum

temperature at the end of 3C discharge was more than that at the end of 4C discharge. During the charge process, the battery temperature demonstrated oscillation and two peaks occurred. The temperature drop during the middle period was the consequence of the heat generated from the battery less than heat absorbed by the PCMs.

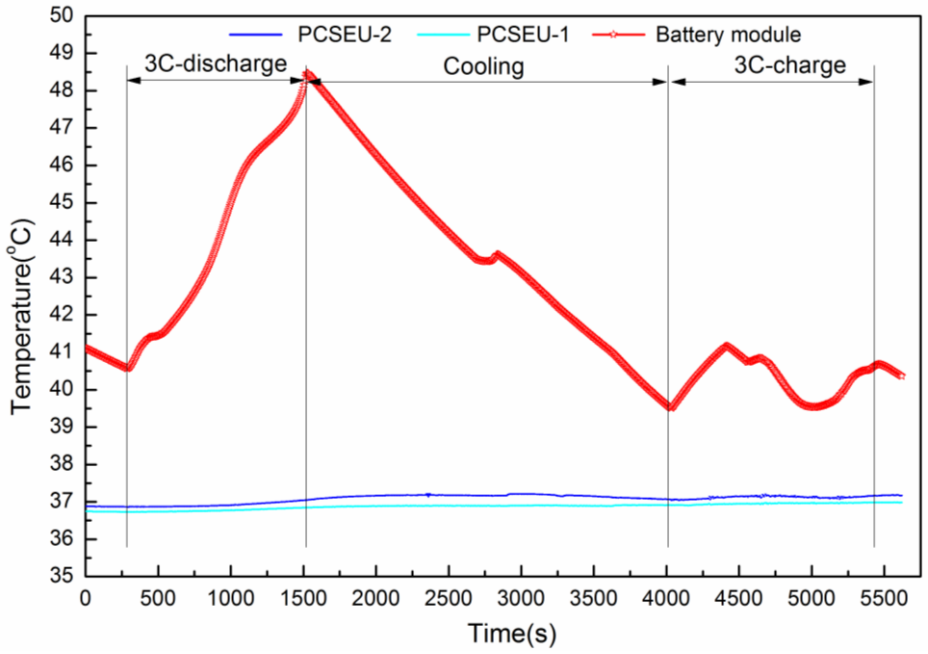

(a) 3C charge/discharge

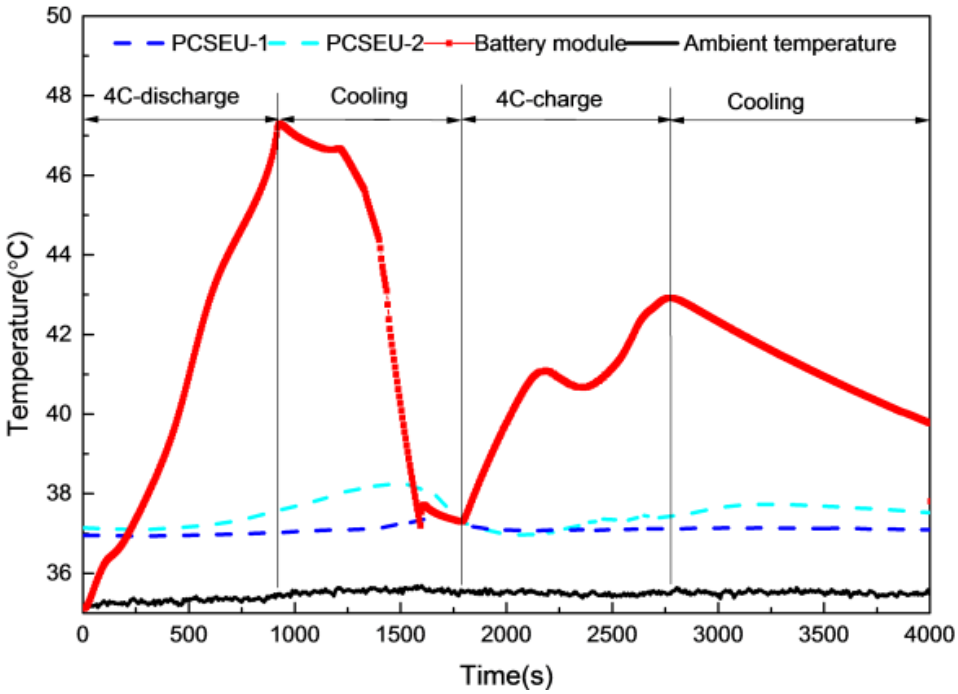

(b) 4C charge/discharge

Fig. 10 Temperature change versus time at 35 °C during 3C and 4C charge/discharge.

For the case of 3C charge and discharge, as illustrated in Fig. 10 (a), the battery maximum

temperature reached 48.5 ^{o}C when the discharge was completed. The temperature rise was 7.9 ^{o}C. During the cooling stage, forced convection with small air flow rate 7 m^3/h was used to cool the battery and the PCSEUs. Since a large amount of heat was stored in the PCMs with latent heat that could not completely dissipate to the cooling air, the initial temperature at 3C charge was 39.5 ^{o}C. During the 3C charge process, the maximum temperature of the battery at the first peak was 41.2 ^{o}C, whereas at the second peak was 40.7 ^{o}C.

From Fig. 10(b), it could be clearly seen that the maximum temperature of the battery pack in the 4C charge and discharge process was 47.4 ^{o}C and 43.0 ^{o}C, respectively. Correspondingly, the temperature rise was 12.4 ^{o}C and 8.0 ^{o}C, respectively. After the 4C discharge was completed, the forced convection cooling with an air flow rate of 40 m^3/h was used to reduce the temperature of the battery and PCSEUs. Owing to insufficient cooling, the initial temperature of the battery was 37.0 ^{o}C at the start of 4C charge. Since the natural convection cooling was used after the 4C charge process, the temperature drop rate was smaller than that under forced convection cooling.

It was well known that the larger the charge and discharge rate, the larger the heat generation of the battery. Consequently, the battery temperature rise at 2C and 3C charge/discharge was far less than that at 4C charge/discharge under the same cooling conditions. Therefore, it could be recognized that the TMS with composite PCM was able to keep the battery temperature below the allowed temperature under ambient temperature of 35 ^{o}C.

4.4.2 Impact of different ambient temperatures

Fig. 11 presents the experimental temperature profiles of the battery and PCSEUs at ambient temperature of 28 ^{o}C and 42 ^{o}C during 4C discharge process. For the case of 28 ^{o}C, as shown in Fig. 11(a), the PCM absorbed the heat by the sensible heat when the phase change temperature is higher than ambient temperature. The initial temperature of the battery pack was nearly the same as the PCM temperature. The maximum temperature of the battery was 43.3 ^{o}C at the end of the discharge. The temperature was slightly lower than 44.2 ^{o}C under natural convection cooling conditions without PCM. The main reason could be that the copper structure of the TMS had a large area of the dissipation and enhanced the natural convection cooling. As a result, the battery temperature dropped. Moreover, less heat absorption of the PCMs in the form of sensible heat led to small temperature drop of the battery pack.

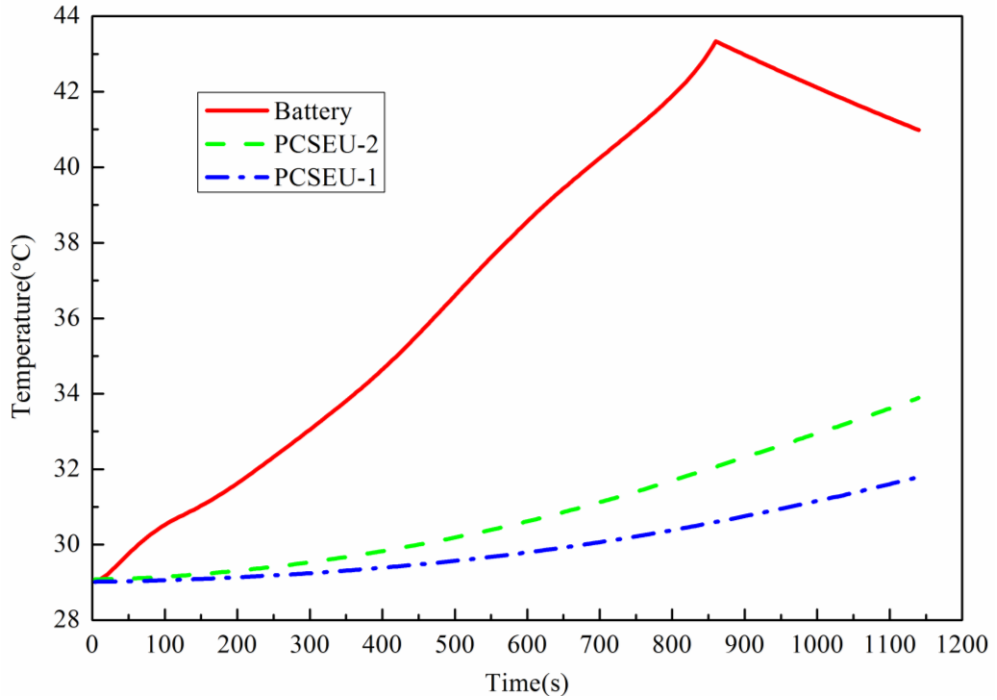

(a) 28℃

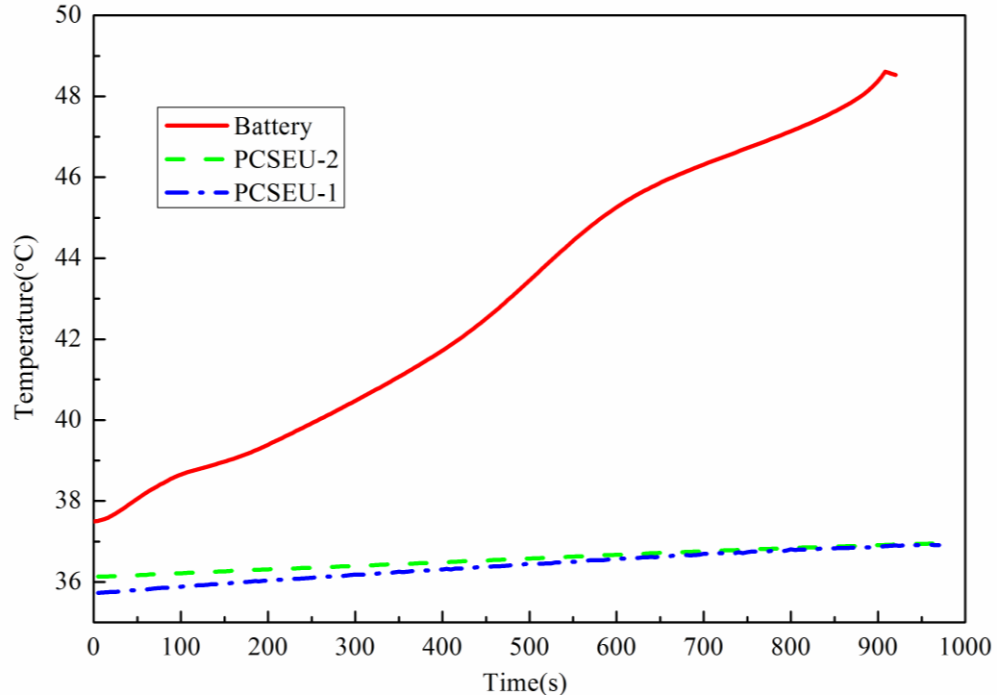

(b) 42℃

Fig. 11 Temperature profile of the battery with the TMS under 28 ºC and 42 ºC

As the ambient temperature was 42 ºC, the PCM absorbed the heat in the form of the latent heat. This caused the initial temperature of the battery was slightly higher than the phase change temperature of the PCM but lower than the ambient temperature, as shown in Fig. 11(b). When the discharge completed, the maximum temperature of the battery was 48.5 ºC, which was lower than the ultimate safe temperature of 55 ºC. This indicated that the composite PCM

based TMS could fully implement its potential for the temperature control of the battery pack as the ambient temperature exceeded phase change temperature.

Comparison of the temperature rise for the battery pack at different ambient temperatures is shown in Figs. 10 and 11. The battery temperature increased 4.1 ^{o}C when the ambient temperature ascended from 28 ^{o}C to 35 ^{o}C. While it increased only 1.1 ^{o}C as the ambient temperature ascended from 35 ^{o}C to 42 ^{o}C. It could be recognized that heat absorption by latent heat or sensible heat resulted in the different the battery temperature rise as increasing the same ambient temperature. Furthermore, the composite PCM based TMS may restrain the fluctuation of the battery temperature caused by the change of ambient temperature.

Additionally, the passive TMS could suffer from a failure in the control of the battery temperature as the PCM completely melted. In order to evaluate the thermal behavior of the battery under such conditions, the temperatures of the battery and PCSEUs under PCM cooling and natural convection cooling conditions are illustrated in Fig. 12. The discharge rate was 4C and the ambient temperature was 35 ^{o}C.

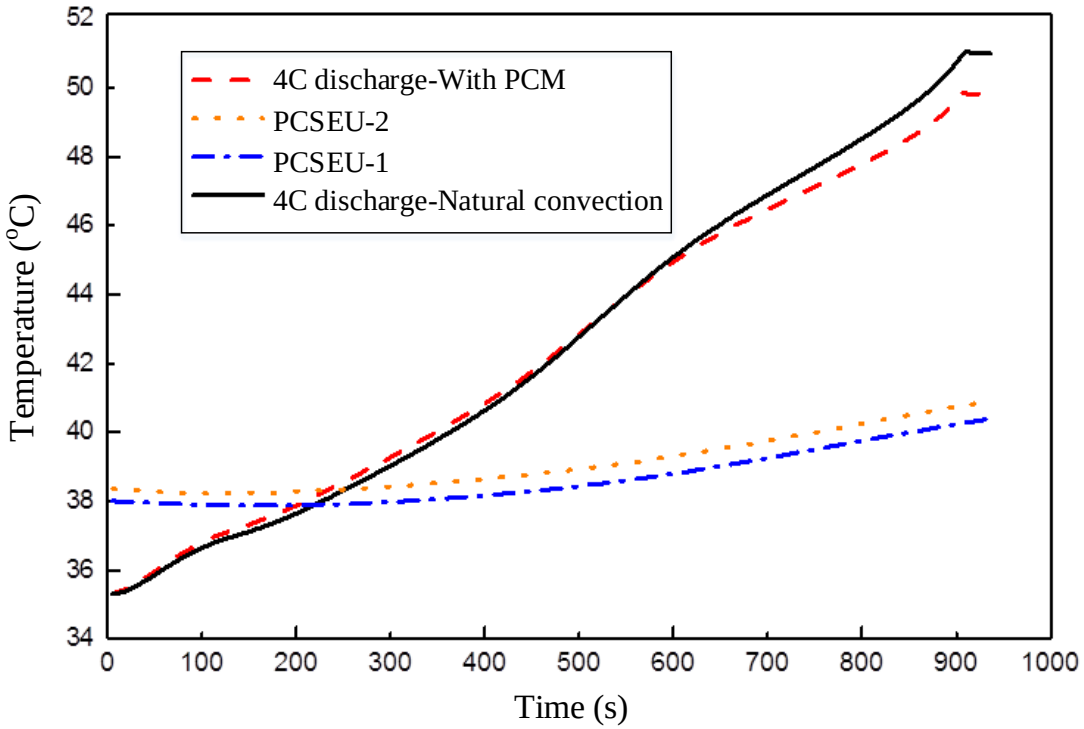

Fig. 12 Temperatures of battery and PCSEUs under PCM and natural convection cooling.

As can be seen from Fig. 12, the PCSEUs temperature was higher than 38 ^{o}C during 4C discharge process, which denoted that the PCM was completely melted. The maximum value of the battery temperature was 50.1 ^{o}C at the end of 4C discharge. Compared with the results

shown in Fig. 10, the battery temperature increased approximate 2.7 ^{o}C. Under natural convection cooling conditions, the maximum temperature of the battery could reach 51.3 ^{o}C, which was slightly higher than that for the case of PCM when fully melting. The battery temperature did not show a dramatic rise since the PCM fully melted. This can be explained by the fact that when the PCMs completely melted, the heat absorbed by the PCM was in the form of sensible heat. Due to small specific heat, the battery temperature went up. The temperature rise was higher than that by latent heat. In addition, the melted PCMs did not directly contact with the battery cell and could not prevent the heat rejected from the battery by natural convection cooling. This relieved the temperature rise of the battery. As a consequence, the proposed structure of the novel TMS improved the thermal performance of the battery pack.

4.5 Thermal performance during charge/discharge cycles

The battery pack underwent a large number of charge and discharge cycles during the actual operating conditions. In order to evaluate the thermal performance of the ACS and novel TMS during charge and discharge cycles, numerical simulations were performed for the battery pack. In the current study, the rates of charge and discharge were set to 4C. The ambient temperature was 35 ^{o}C. The cooling time between charge and discharge process was set to 10 minutes. The initial temperature of the battery and the PCM were set to 35 ^{o}C. For the novel TMS, The natural convection cooling with heat transfer coefficient of 5 W/(m^{2}·K) was used during the cooling process. For the ACS, the air flow rate was 100 m^{3}/h and 200 m^{3}/h, respectively. The battery pack was cooled by the forced convection between the charge and discharge process. Fig. 13 illustrates the profiles of the maximum temperature and temperature difference of the battery pack as well as the liquid fraction of the PCM for the ACS and novel TMS.

As shown in Fig. 13(a), when the air flow rate was 100 m^{3}/h, the maximum temperature of the battery pack was 49.5 ^{o}C in the first charge-discharge cycle process. However, in the second 4C discharge process, the maximum temperature of the battery reached to 56 ^{o}C, which exceeded the highest allowable temperature. During the whole cycles, the maximum temperature difference was increasing and the largest value of 5.9 ^{o}C is achieved. In the discharge process, the temperature difference ascended rapidly. When the air flow rate was 200 m^{3}/h, the battery maximum temperature arrived at 49.0 ^{o}C at the end of the second 4C discharge and the temperature rise was 14.0 ^{o}C although the battery operated in the safe

temperature range during both cycles. There was a rapid increase in temperature difference during the two discharge processes. During the first charge process it ascended but descended during the second charge process. It also descended in the second cooling stage and second discharge initial stage. The maximum temperature difference reached 3.8 ºC after the second discharge ends. Additionally, the battery could not be cooled enough before the beginning of the second cycle under the conditions of 100 m^3/h and 200 m^3/h. For the case of 42 ºC and 200 m^3/h, the battery temperature also exceeded the safety temperature, which was not shown in Fig. 13(a).

According to the above results, an air flow rate below 200 m^3/h could not meet the requirement of the battery temperature control for the ACS. Furthermore, the larger the air flow rate, the better the cooling performance. However, the increase of the air flow rate not only led to a poor temperature uniformity of the battery pack but also increased the pressure difference, which significantly increased the power consumption of the cooling fan. It was proved that the air cooling way would reduce the battery energy efficiency.

As can be seen from Fig. 13(b), the maximum temperature ascended with the increase of the charge/discharge cycle. For each charge/discharge cycle, the battery temperature reached the maximum value at the end of the discharge. At the end of the fourth discharge, the battery temperature reached the maximum value of 56.9 ºC, which exceeded the highest allowable temperature. During the former three discharge processes, the maximum temperature of the battery pack was 44.2 ºC, 48.3 ºC and 52.0 ºC, respectively. The battery temperature increased approximately 4.0 ºC after each cycle. During all the 4C charge processes, it could be seen that there were two temperature peaks. The second peak was approximately 0.8 ºC higher than the first peak for each charge process. The battery temperature drop in the charge process was the consequence of the heat dissipation more than the heat generation of the battery. During three charge processes, the battery maximum temperature was 43.6 ºC, 46.4 ºC and 51.6 ºC, respectively. Correspondingly, the battery temperature increased 2.8 ºC and 5.2 ºC, respectively. Since the battery was cooled by the latent heat of the PCMs, the battery temperature difference was extremely small.

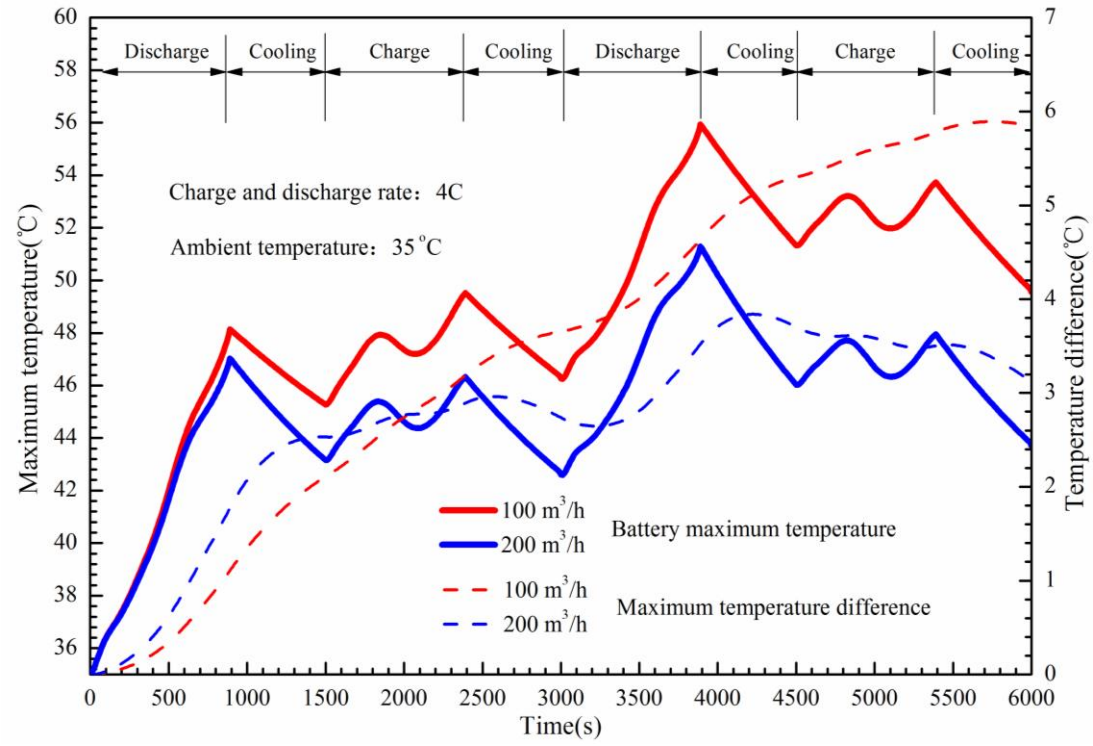

(a) Battery maximum temperature and temperature difference for ACS

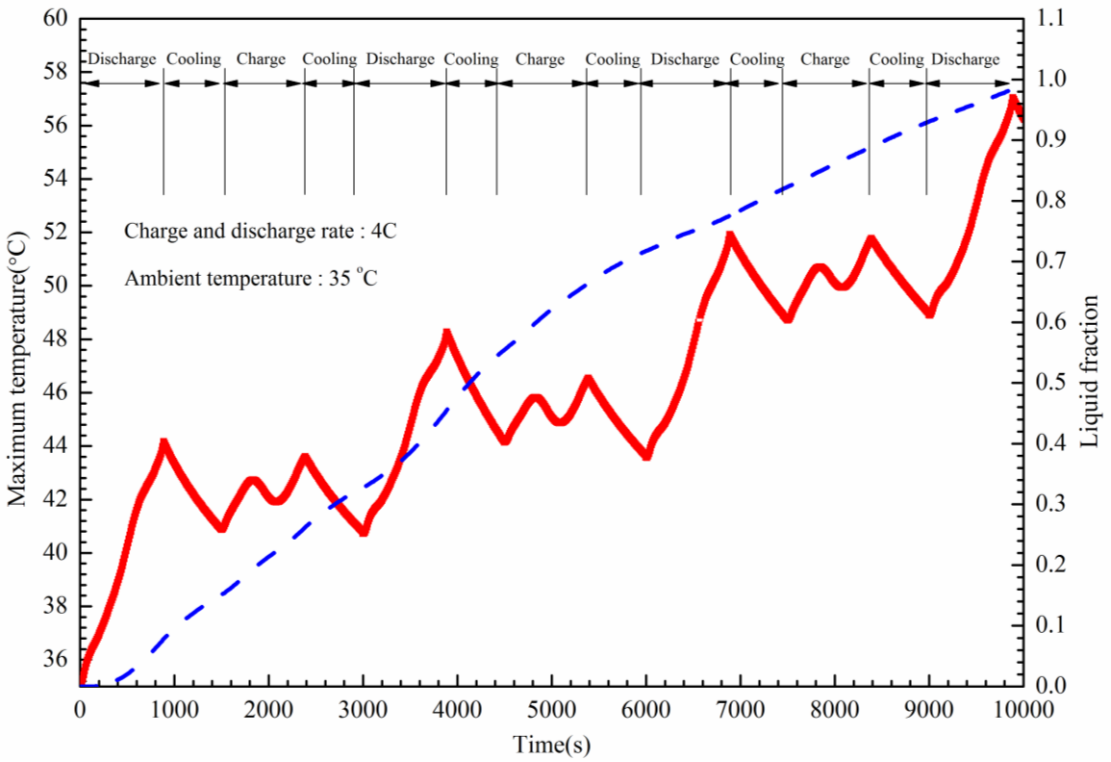

(b) Battery maximum temperature and liquid fraction for novel TMS

Fig. 13 Profiles of battery maximum temperature, temperature difference and liquid fraction for ACS and novel TMS during 4C charge/discharge cycle

As a result of the cooling not being high enough after each discharge or charge process, the

initial temperature of the battery in the next cycle ascended. Moreover, the larger initial temperature of the battery plays a negative role in the battery rise [30]. Therefore, this resulted in a higher temperature rise during the charge and discharge cycles. In addition, it could be also seen from Fig. 13(b) that the liquid fraction of the PCM increased during the cycles. Since the surface temperature of the battery was more than the phase transition temperature during the cooling processes, the PCSEUs were still constantly absorbing the heat generated by the battery. As a consequence, the liquid fraction of the PCM enlarged during cooling process. Finally, the value of the liquid fraction reached 1.0, which means that all of the PCMs inside the PCSEUs were fully melted.

It was worth noting that if an external power supply was available, the auxiliary air cooling could be used to increase the working time of the PCM during charge and cooling period. Under such conditions, the battery pack with the passive TMS had the maximum energy efficiency. Moreover, if the battery and the PCM were fully cooled to the desirable temperature (here was 35 ^{o}C), the battery temperature would be well controlled and the PCM would be available for infinite recycling.

5. Conclusions

A novel passive TMS based on the copper foam and paraffin composite PCM for a lithium-ion power battery was designed and the thermal performance of the battery pack was investigated both experimentally and numerically. The impacts of several control parameters such as the PCSEU casing, effective thermal conductivity of composite PCM, different geometric structure parameters, ambient temperature and charge/discharge rate on the battery temperature were analyzed in a systematic manner. Thermal performance of the battery pack during charge/discharge cycles was simulated. Major findings based on the experimental and numerical results were as follows:

(1) The external casing of the PCM remarkably improved the heat absorption efficiency of the PCSEU-2, but had insignificant effect on the efficiency of the PCSEU-1 with relative large thermal resistance to the battery cell. The large thermal conductivity of the PCM could lead to good temperature homogeneity in the melting process but a further increase could not significantly reduce the battery temperature.

(2) The heat conducting sheet thickness had the largest impact on the battery temperature, followed by the connecting fin height, fin thickness and collector plate thickness. Reducing the thermal resistance of the heat conducting sheet could be the most effective way to improve the thermal performance of the TMS.

(3) The highest temperature of the battery pack with the passive TMS at 3C and 4C rates charge/discharge could be maintained within the safety temperature under 28 ^{o}C, 35 ^{o}C and 42 ^{o}C respectively. The composite PCM could perform better temperature control capability at high ambient temperature. The indirect contact between the PCM and battery cell avoided heating the battery as the PCM entirely melted.

(4) Pure ACS with an air flow rate ≤200 m^3/h could not meet the requirement of the battery temperature control. It would significantly consume more battery power and led to much higher temperature difference. The novel TMS could achieve up to 3 cycles of 4C charge and discharge at 35 ^{o}C while keeping the maximum temperature of the battery pack below 52 ^{o}C. Decreasing initial temperature of the battery during charge/discharge cycles could be the key to improve the cycle thermal performance.

Acknowledgement

The authors would like to acknowledge the financial support from University of Hertfordshire, United Kingdom. This work was supported by the CRRC TANGSHAN CO., LTD.

References

[1] Hannan M A, Lipu M S H, Hussain A, Mohamed A. A review of lithium-ion battery state of charge estimation and management system in electric vehicle applications: Challenges and recommendations. Renewable and Sustainable Energy Reviews 2017; 78: 834-854.

[2] Liu H, Wei Z, He W, Zhao J. Thermal issues about Li-ion batteries and recent progress in battery thermal management systems: A review. Energy Conversion and Management, 2017, 150: 304-330.

[3] Effat M B, Wu C, Ciucci F. Modeling efforts in the key areas of thermal management and safety of lithium ion battery cells: a mini review. Asia‐Pacific Journal of Chemical

Engineering 2016; 11(3): 399-406.

[4] Abada S, Marlair G, Lecocq A, Petit M, Sauvant-Moynot V, Huet F. Safety focused modeling of lithium-ion batteries: A review. Journal of Power Sources 2016; 306: 178-192.

[5] Xia G, Cao L, Bi G. A review on battery thermal management in electric vehicle application. Journal of Power Sources, 2017, 367: 90-105.

[6] Wang T, Tseng K J, Zhao J, Wei Z. Thermal investigation of lithium-ion battery module with different cell arrangement structures and forced air-cooling strategies. Applied energy 2014; 134: 229-238.

[7] Saw L H, Ye Y, Tay A A O, Chong W T, Kuan S H, Yew M C. Computational fluid dynamic and thermal analysis of Lithium-ion battery pack with air cooling. Applied Energy 2016; 177: 783-792.

[8] Li K, Yan J, Chen H, Wang Q. Water cooling based strategy for lithium ion battery pack dynamic cycling for thermal management system. Applied Thermal Engineering, 2018, 132: 575-585.

[9] Liu R, Chen J, Xun J, Jiao K, Du Q. Numerical investigation of thermal behaviors in lithium-ion battery stack discharge. Applied Energy, 2014, 132: 288-297.

[10] Zhang S, Zhao R, Liu J, Gu J. Investigation on a hydrogel based passive thermal management system for lithium ion batteries. Energy, 2014, 68: 854-861.

[11] M. Malik, I. Dincer, M. A. Rosen. Review on use of phase change materials in battery thermal management for electric and hybrid electric vehicles. International Journal of Energy Research 2016; 40 (8):1011-1031.

[12] Li W Q, Qu Z G, He Y L, Tao Y B. Experimental study of a passive thermal management system for high-powered lithium ion batteries using porous metal foam saturated with phase change materials. Journal of Power Sources, 2014, 255: 9-15.

[13] Wu W, Yang X, Zhang G, Ke X, Wang Z, Situ W, Li X, Zhang J. An experimental study of thermal management system using copper mesh-enhanced composite phase change materials for power battery pack. Energy, 2016, 113: 909-916.

[14] Samimi F, Babapoor A, Azizi M, Karimi G. Thermal management analysis of a Li-ion battery cell using phase change material loaded with carbon fibers. Energy, 2016, 96: 355-371.

[15] Jankowski N R, McCluskey F P. A review of phase change materials for vehicle component thermal buffering, Applied Energy, 2014, 113: 1525-1561.

[16] Farid M M, Khudhair A M, Razack S A K, Al-Hallaj S. A review on phase change energy storage: materials and applications, Energy conversion and management, 2004, 45(9): 1597-1615.

[17] An Z, Jia L, Ding Y, Dang C, Li X. A review on lithium-ion power battery thermal management technologies and thermal safety. Journal of Thermal Science 2017; 26(5): 391-412.

[18] Al-Hallaj S, Selman J R. Thermal modeling of secondary lithium batteries for electric vehicle/hybrid electric vehicle applications. Journal of power sources 2002; 110(2): 341-348.

[19] Karimi G, Azizi M, Babapoor A. Experimental study of a cylindrical lithium ion battery thermal management using phase change material composites. Journal of Energy Storage, 2016, 8: 168-174.

[20] Hussain A, Tso C Y, Chao C Y H. Experimental investigation of a passive thermal management system for high-powered lithium ion batteries using nickel foam-paraffin composite. Energy 2016; 115: 209-218.

[21] Zhong G, Zhang G, Yang X, Li X, Wang Z, Yang C, Yang C, Gao G. Researches of composite phase change material cooling/resistance wire preheating coupling system of a designed 18650-type battery module. Applied Thermal Engineering, 2017, 127: 176-183.

[22] Lv Y, Yang X, Li X, Zhang, G, Wang, Z, Yang, C. Experimental study on a novel battery thermal management technology based on low density polyethylene-enhanced composite phase change materials coupled with low fins. Applied Energy 2016; 178: 376-382.

[23] Sabbah Rami, Kizilel R, Selman J R, Al-Hallaj S. Active (air-cooled) vs passive (phase change material) thermal management of high-power Li-ion packs：Limitation of temperature rise and uniformity of temperature distribution. Journal of Power Sources 2008; 182: 630-638.

[24] Wang Z, Zhang Z, Jia L, Yang L. Paraffin and paraffin/aluminum foam composite phase change material heat storage experimental study based on thermal management of Li-ion battery. Applied Thermal Engineering 2015; 78: 428-436.

[25] Wu W, Wu W, Wang S. Thermal optimization of composite PCM based large-format lithium-ion battery modules under extreme operating conditions. Energy Conversion and Management, 2017, 153: 22-33.

[26] Situ W, Zhang G, Li X, Yang X, Wei C, Rao M, Wang Z, Wang C, Wu W. A thermal management system for rectangular $LiFePO_4$ battery module using novel double copper mesh-enhanced phase change material plates. Energy 2017, 141:613-623.

[27] Alipanah M, Li X. Numerical studies of lithium-ion battery thermal management systems using phase change materials and metal foams, International Journal of Heat and Mass Transfer, 2016, 102: 1159-1168.

[28] Malik M, Dincer I, Rosen M, Fowler M. Experimental investigation of a new passive thermal management system for a li-Ion battery pack using phase change composite material. Electrochimica Acta 2017, 257: 345-355.

[29] Zhao R, Gu J, Liu J. Optimization of a phase change material based internal cooling system for cylindrical Li-ion battery pack and a hybrid cooling design. Energy, 2017, 135: 811-822.

[30] Y. He. Rapid thermal conductivity measurement with a hot disk sensor: Part 1. Theoretical considerations. Thermochimica Acta 2005; 436: 122-129.

[31] Bernardi D, Pawlikowski E, Newman J. A general energy balance for battery systems. Journal of the Electrochemical Society 1984; 132(1):5-12.

[32] Nazari A, Farhad S. Heat generation in lithium-ion batteries with different nominal capacities and chemistries. Applied Thermal Engineering, 2017, 125: 1501-1517.

[33] Shi S, Xie Y, Li M, Yuan Y, Yu J, Wu H, Liu B, Liu N. Non-steady experimental investigation on an integrated thermal management system for power battery with phase change materials. Energy Conversion and Management 2017; 138: 84-96.

[34] Hosseini M J, Rahimi M, Bahrampoury R. Experimental and computational evolution of a shell and tube heat exchanger as a PCM thermal storage system. International Communications in Heat and Mass Transfer 2014; 50: 128-136.

[35] Tiari S, Qiu S, Mahdavi M. Numerical study of finned heat pipe-assisted thermal energy storage system with high temperature phase change material. Energy Conversion and Management 2015; 89: 833-842.

[36] Rao Z, Wang Q, Huang C. Investigation of the thermal performance of phase change material/mini-channel coupled battery thermal management system. Applied Energy 2016; 164: 659-669.

[37] Tan F L, Hosseinizadeh S F, Khodadadi J M, Fan L. Experimental and computational study of constrained melting of phase change materials (PCM) inside a spherical capsule. International Journal of Heat and Mass Transfer 2009; 52(15): 3464-3472.

[38] Wu W, Yang X, Zhang G, Chen K, Wang S. Experimental investigation on the thermal performance of heat pipe-assisted phase change material based battery thermal management system. Energy Conversion and Management 2017; 138: 486-492.

[39] Rao Z H, Wang S F, Zhang Y L. Simulation of heat dissipation with phase change material for cylindrical power battery. Journal of the Energy Institute 2012; 85(1): 38-43.